Electronic Supplementary Information

for

Polymorphism and spin crossover in mononuclear Fe^{II} species containing new dipyridylamino-substituted s-triazine ligands

Tamsyn M. Ross,[a] Boujemaa Moubaraki,[a] Suzanne M. Neville,[a] Stuart R. Batten[a] and Keith S. Murray*[a]

[a] School of Chemistry, Building 23, Monash University, Clayton, Victoria 3800, Australia, Fax: +61-3-99054597 E-mail: keith.murray@monash.edu

Table of Contents

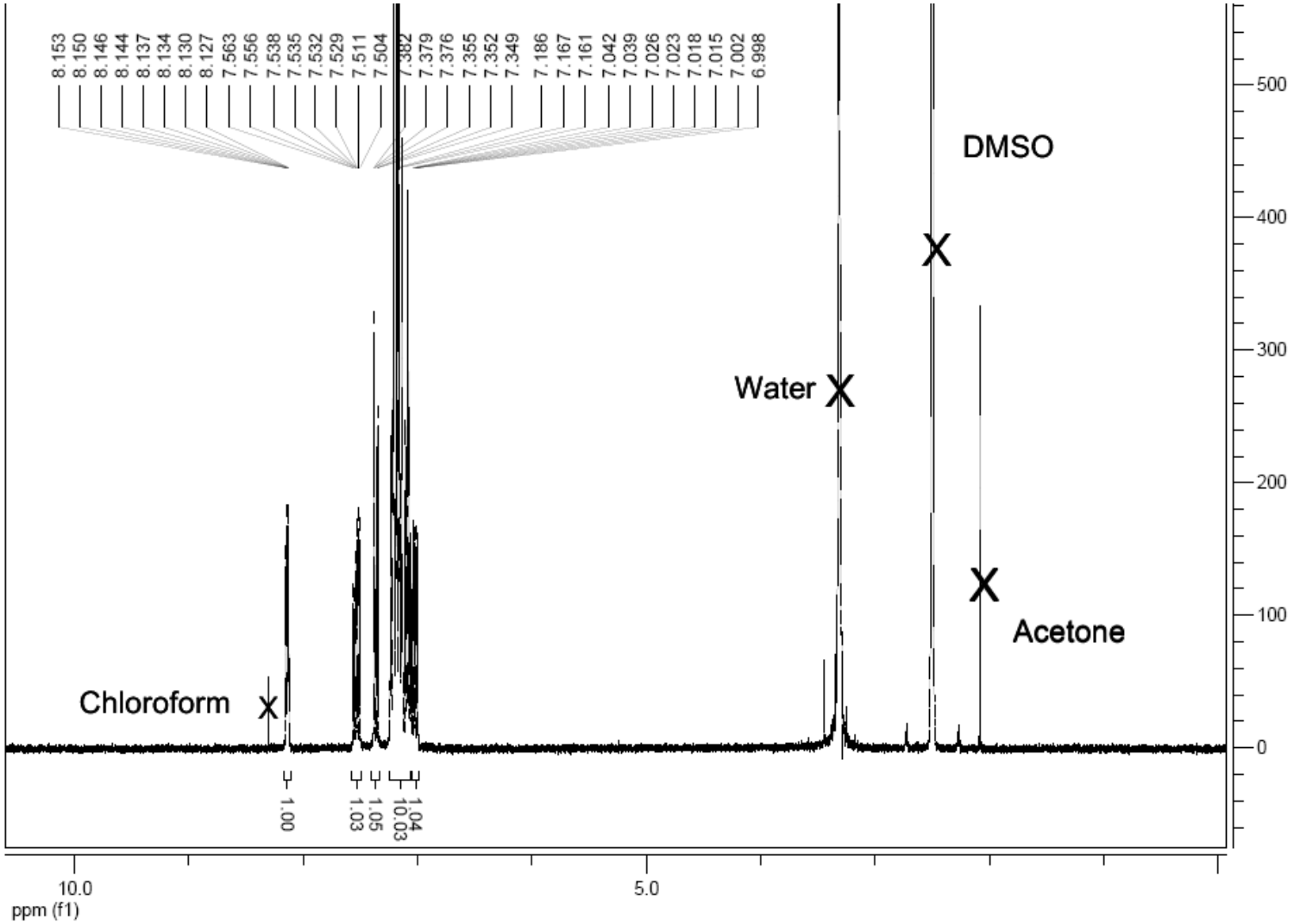

Figure S1 ^{1}H NMR of DDT.

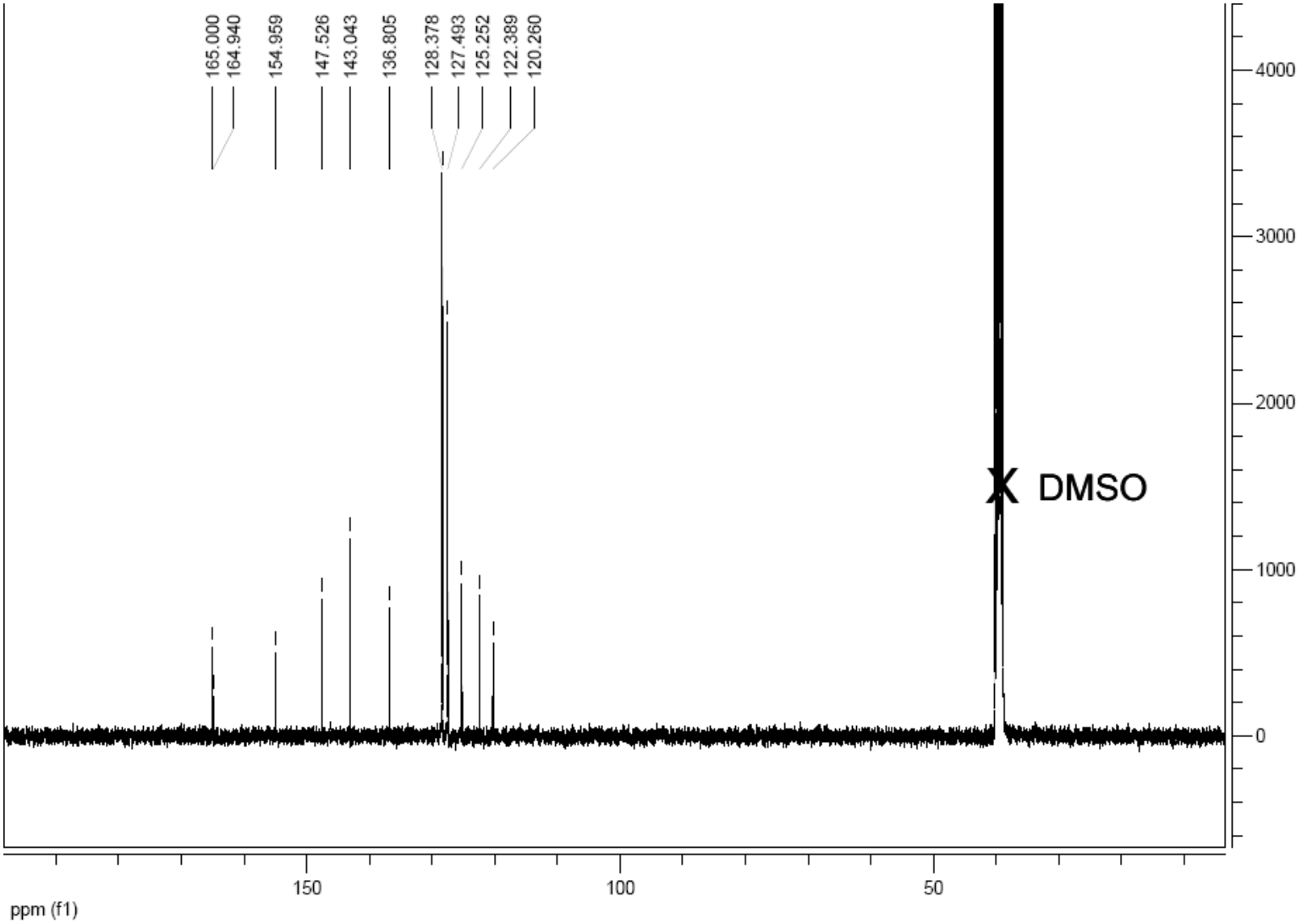

Figure S2 ^{13}C NMR of DDT.

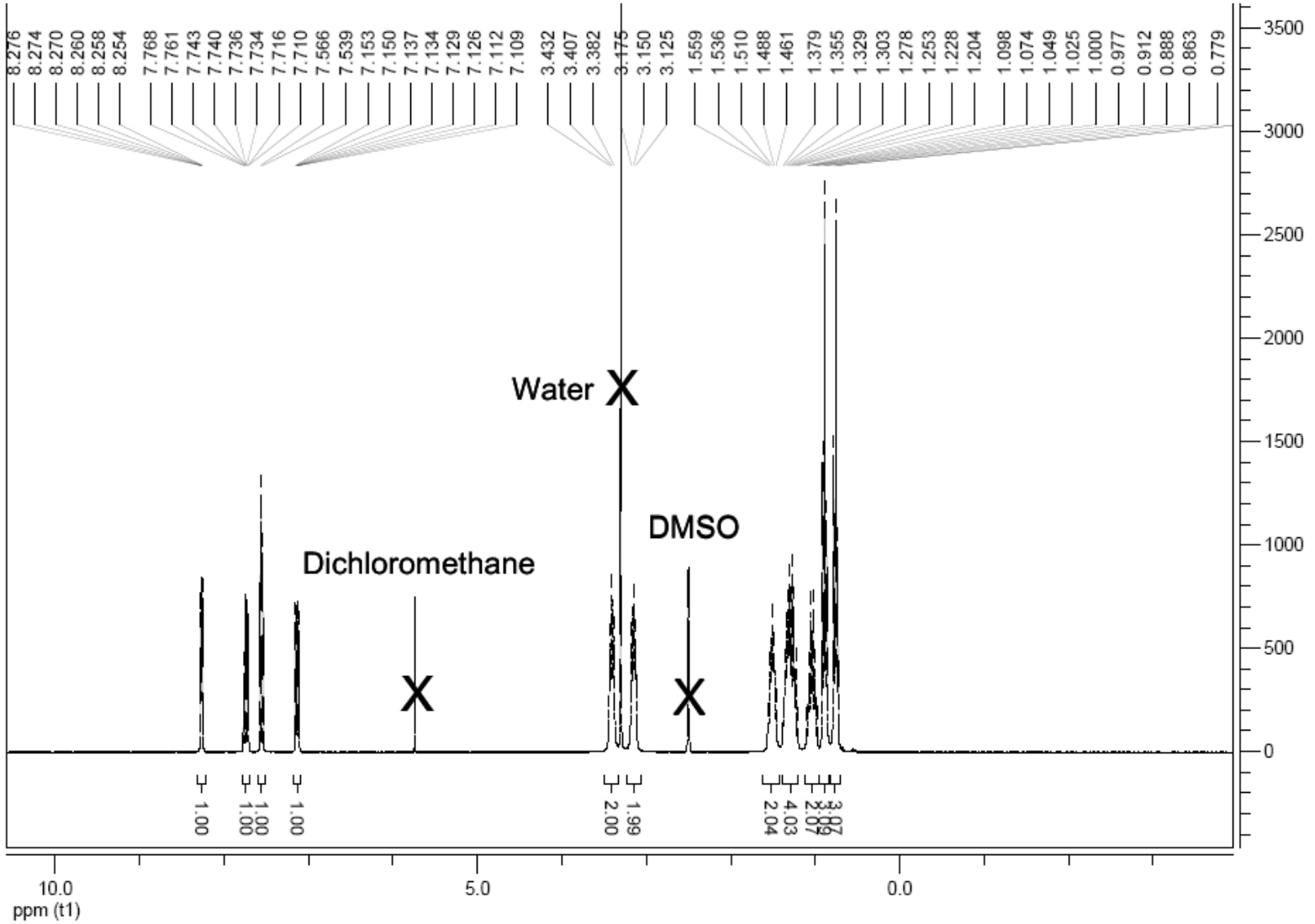

Figure S3 ^{1}H NMR of DDB.

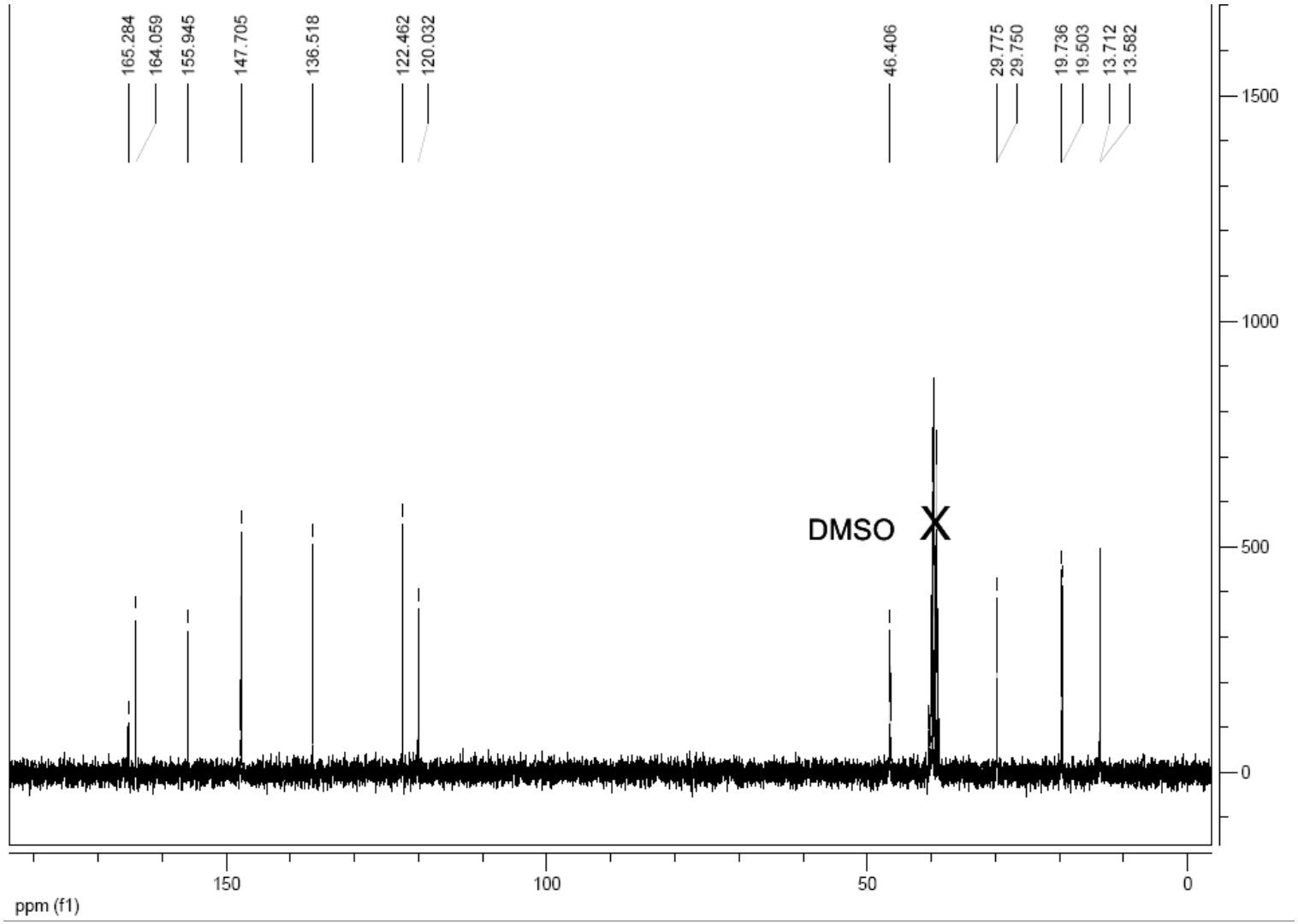

Figure S4 ^{13}C NMR of DDB.

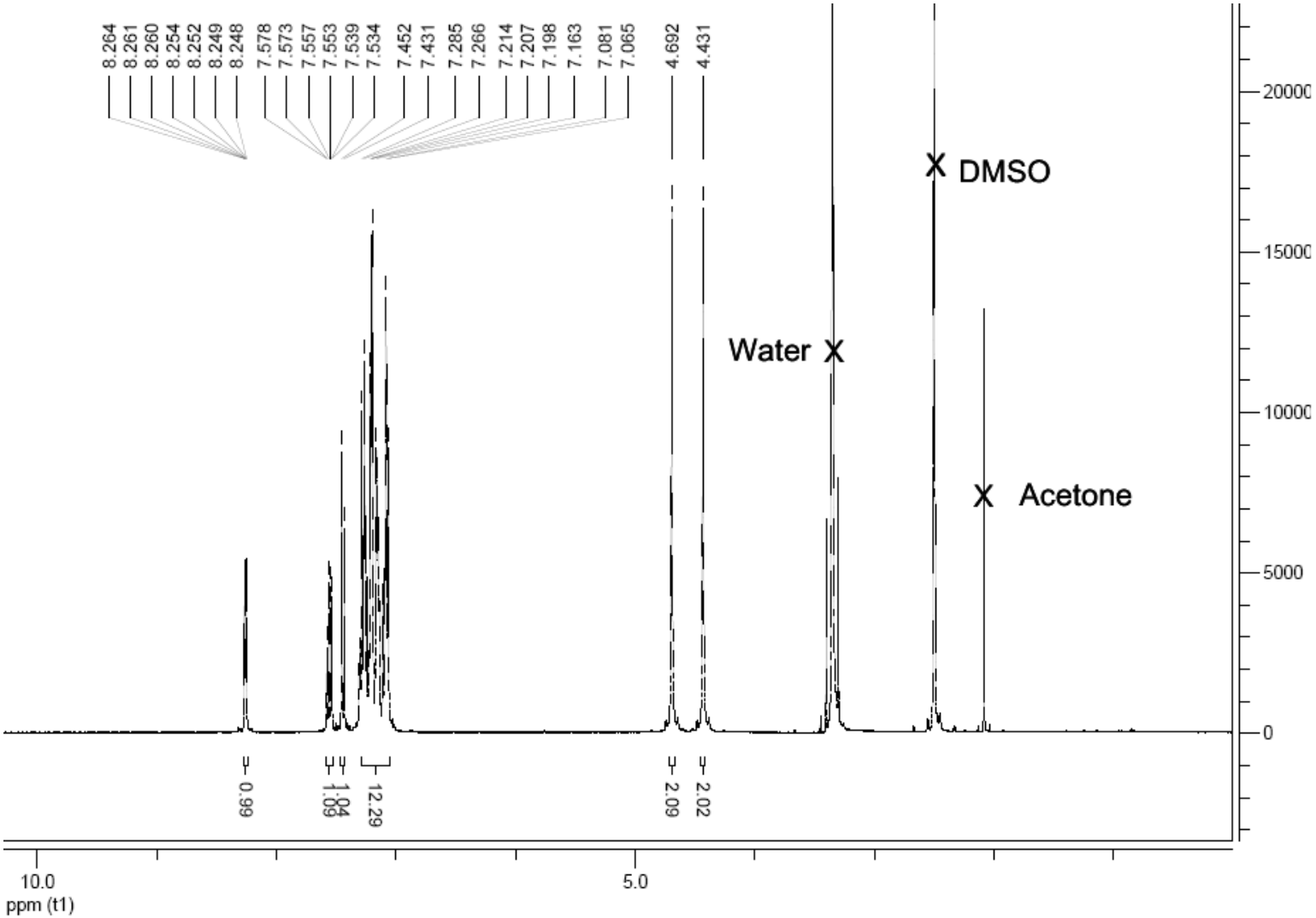

Figure S5 ^{1}H NMR of DBB.

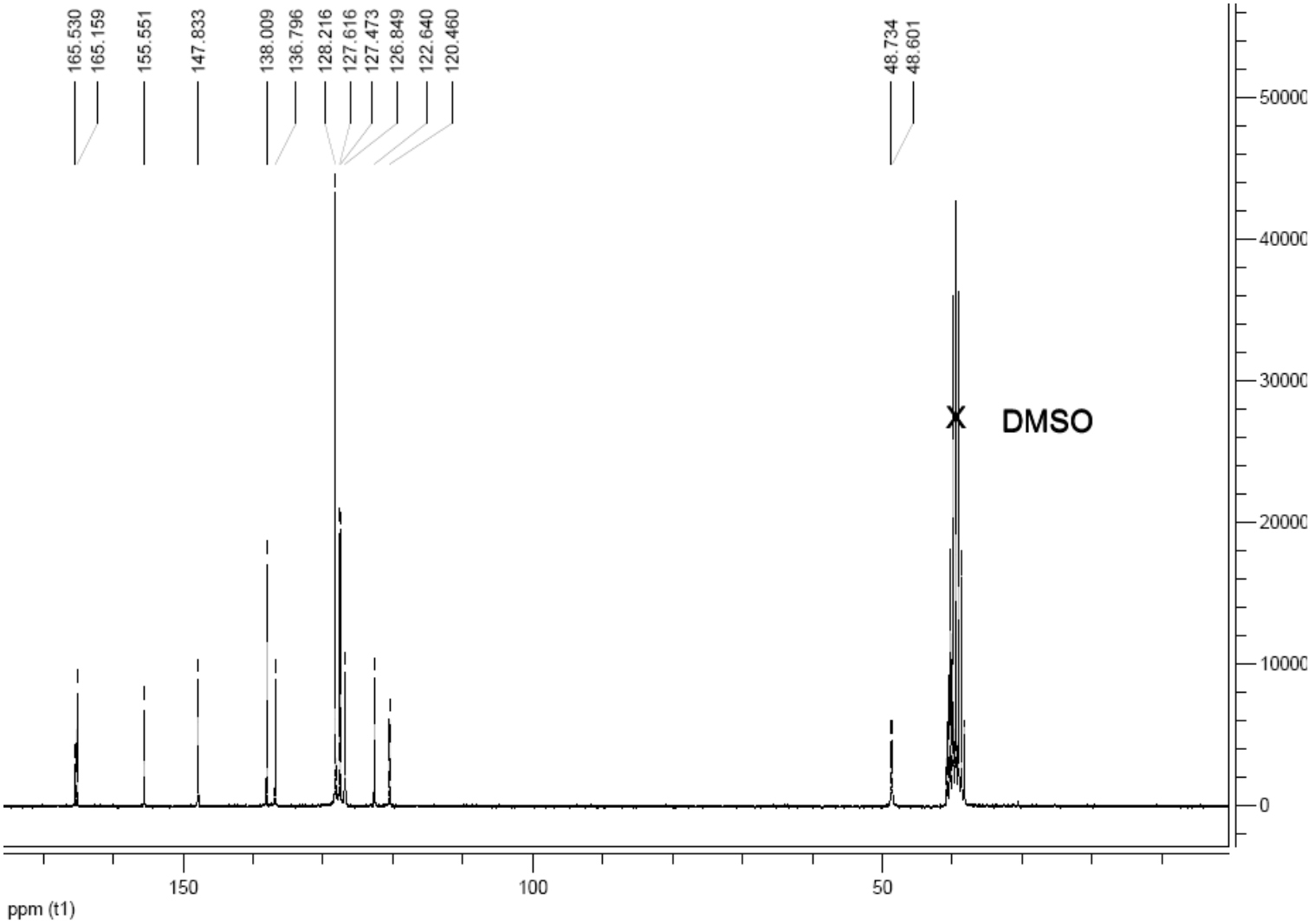

Figure S6 ^{13}C NMR of DBB.

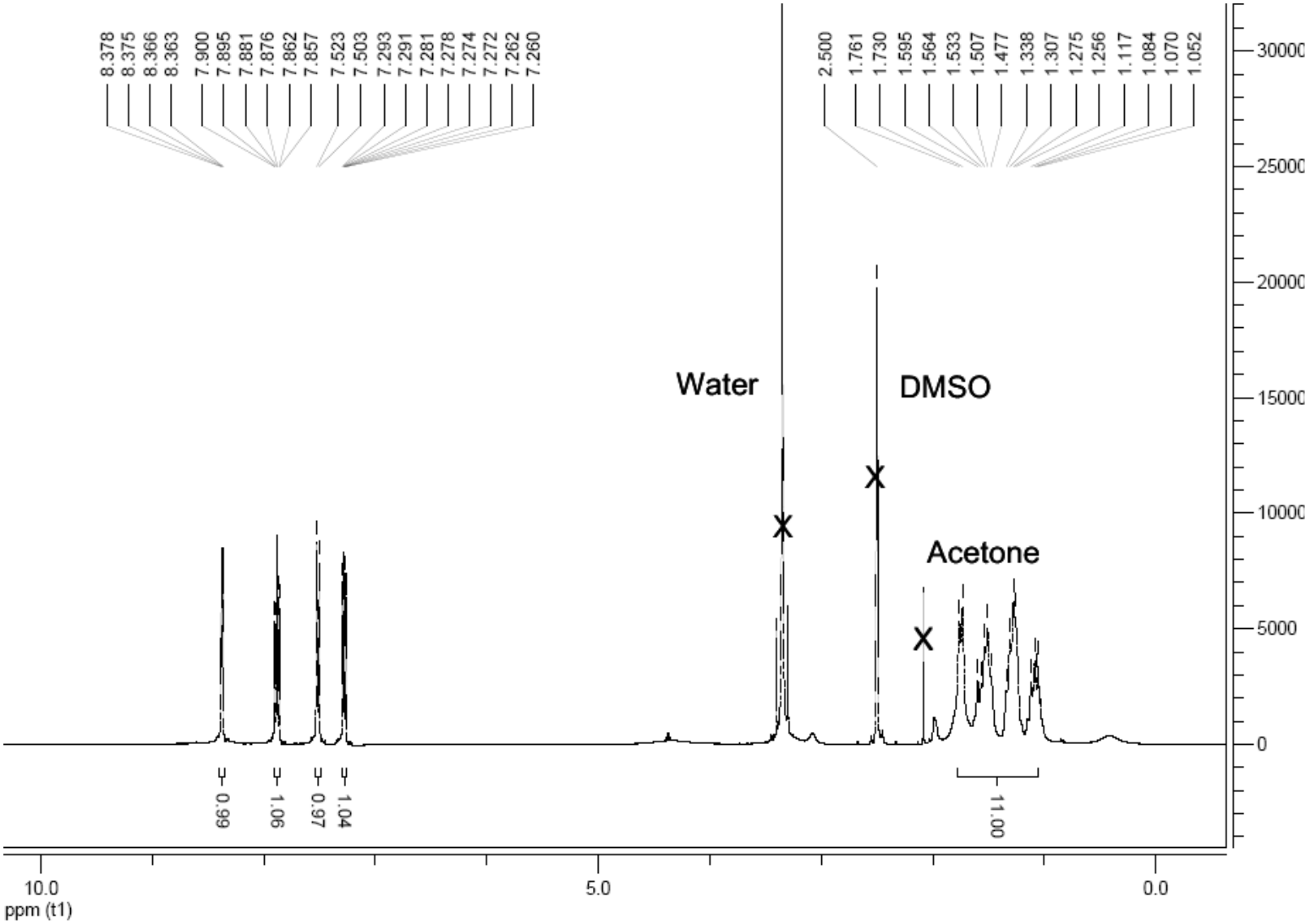

Figure S7 ^{1}H NMR of DCCl.

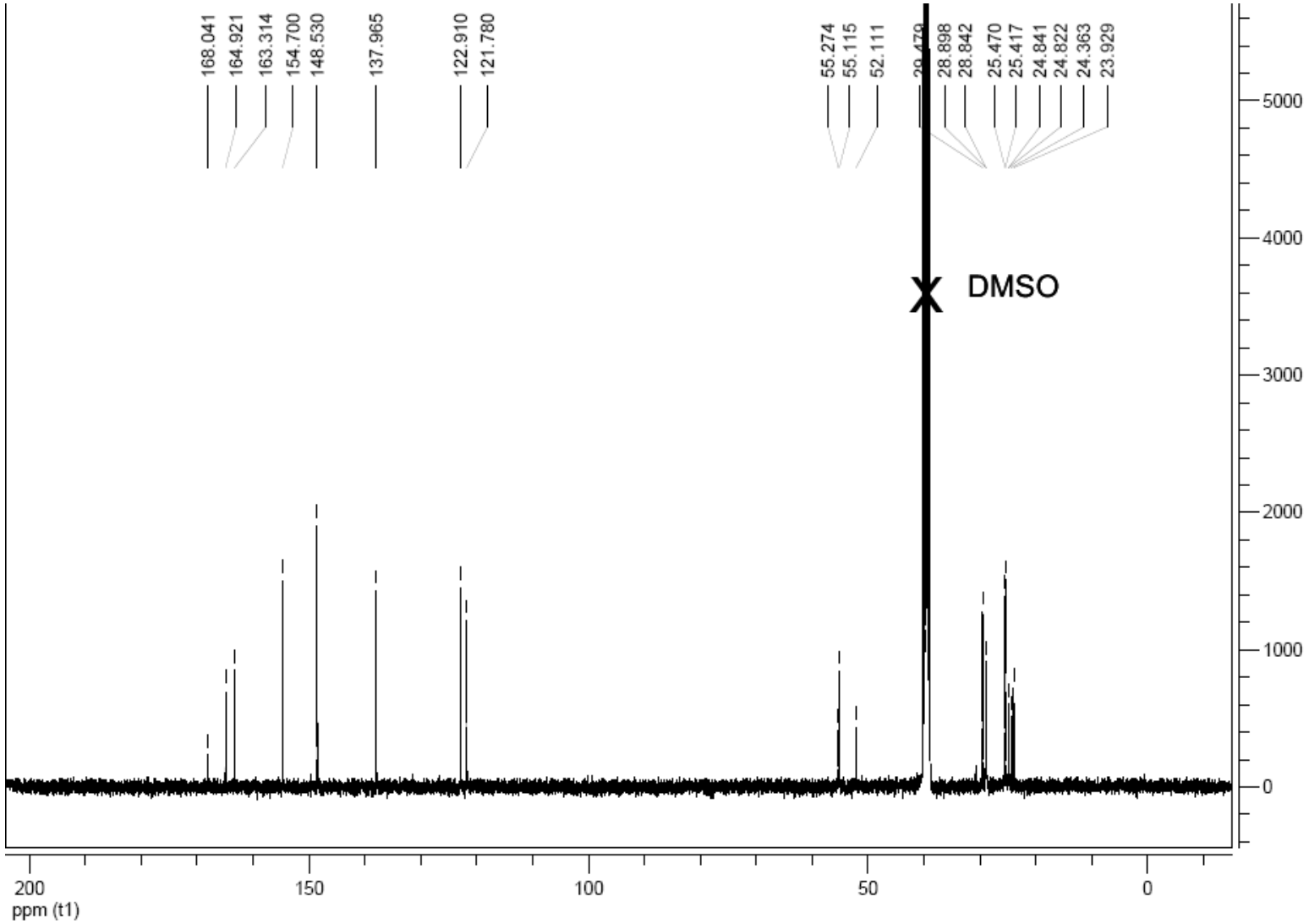

Figure S8 ^{13}C NMR of DCCl.

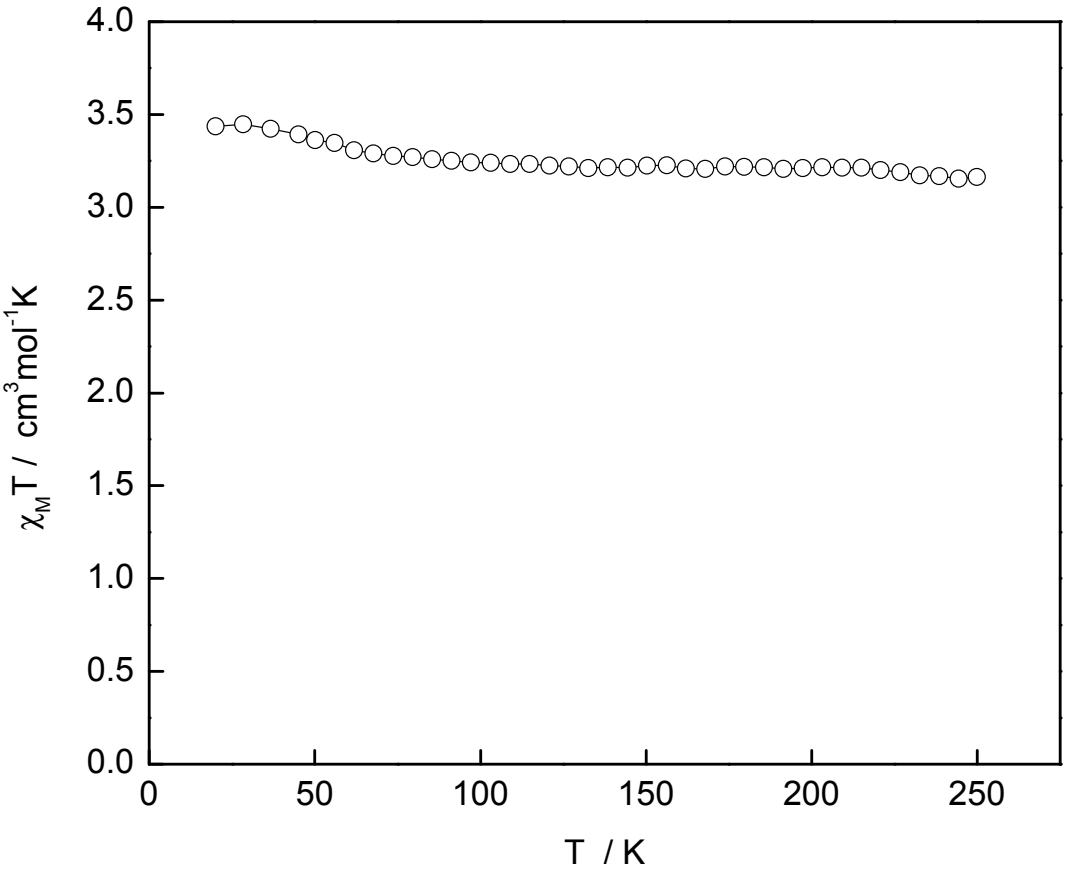

Figure S9 Magnetic susceptibility ($\chi_M T$) plot for **7** (*trans*-[$Fe^{II}(NCS)_2(DDT)_2$]•$4CH_2Cl_2$).

Special Refinement Details for Crystal Structures 2, 3, 4, 5, 9 and 10

Data for **1a**, **1b**, **2** and **5** were collected at the Australian Synchrotron. Collection to high 2θ values was not always possible using this set-up resulting in low data completeness in some cases (> ~93 %). In all instances, however, the data-to-parameter ratios remain very good, and connectivity of the main moieties is unambiguous.

2: Plate-shaped crystals of **2** were extremely thin, resulting in a large number of overloaded reflections during data collection. Crystals of **2** consisted of heavily inter-grown orange plates, and although a significant effort was made to select a good quality crystal, many crystals tried were found to be badly twinned. The current data set was the best that could be

obtained with the samples available. Thus, the relatively high R-factor observed here is a result of poor crystal quality. ISOR restraints have been applied to Fe1, C2, C3, C6, C12, C15, C17, C36, C8, C9, C10, C11, C26, C27, C28, N1, N2 and N3. Data were collected using the shortest wavelength available and the shortest crystal-detector distance with a phi-stage. Collection to high 2θ values was not possible using this set-up resulting in low data completeness. However, the data-to-parameter ratio remains very good.

3: The crystal structure of **3** contains a disordered ethanol molecule that has been modelled in three parts. All atoms within the disordered ethanol molecule have been refined isotropically. Within this disordered ethanol molecule, C44C and C45C have been constrained to have the same isotropic thermal parameters, C44A and C44B have been constrained to have the same isotropic thermal parameters, C45A and C45B have been constrained to have the same isotropic thermal parameters, and O1A and O1B have been constrained to have the same isotropic thermal parameters. The atoms O1A and O1B, and the atoms C45A and C45B, have been constrained to occupy the same XYZ coordinates as each other. The distance between O1C and C45C has been restrained to 2.45(1) Å. Hydrogen atoms have not been assigned to the disordered ethanol molecule. A possible hydrogen bond between N11 and O1A (as the donor atom) is noted, thus occurring between the highly disordered ethanol molecule and a nitrogen atom within the dicyanamide ligand.

4: The crystal structure of **4** contains positional disorder in one of the dibutylamine ligand substituents; that is, carbon atoms C15, C16, C17 and C18 are disordered over two positions in a ratio of 60% (part A) to 40% (part B). An ISOR restraint has been applied to the methanol oxygen atom O1.

5: The crystal structure of **5** contains a small amount of disorder in one of the dibutylamine ligand substituents; that is, carbon atoms 46 and 47 are disordered over two positions in a ratio of 75% (part A) to 25% (part B). SADI restraints have been applied to the atom pairs C45/C46A and C45/C46B, as well as to the atom pairs C46A/C47A and C46B/C47B. An ISOR restraint has been used on C47B. Data were collected using the shortest wavelength available and the shortest crystal-detector distance with a phi-stage. Collection to high 2θ values was not possible using this set-up resulting in low data completeness. However, the data-to-parameter ratio remains very good.

8: An ISOR restraint has been applied to C7.

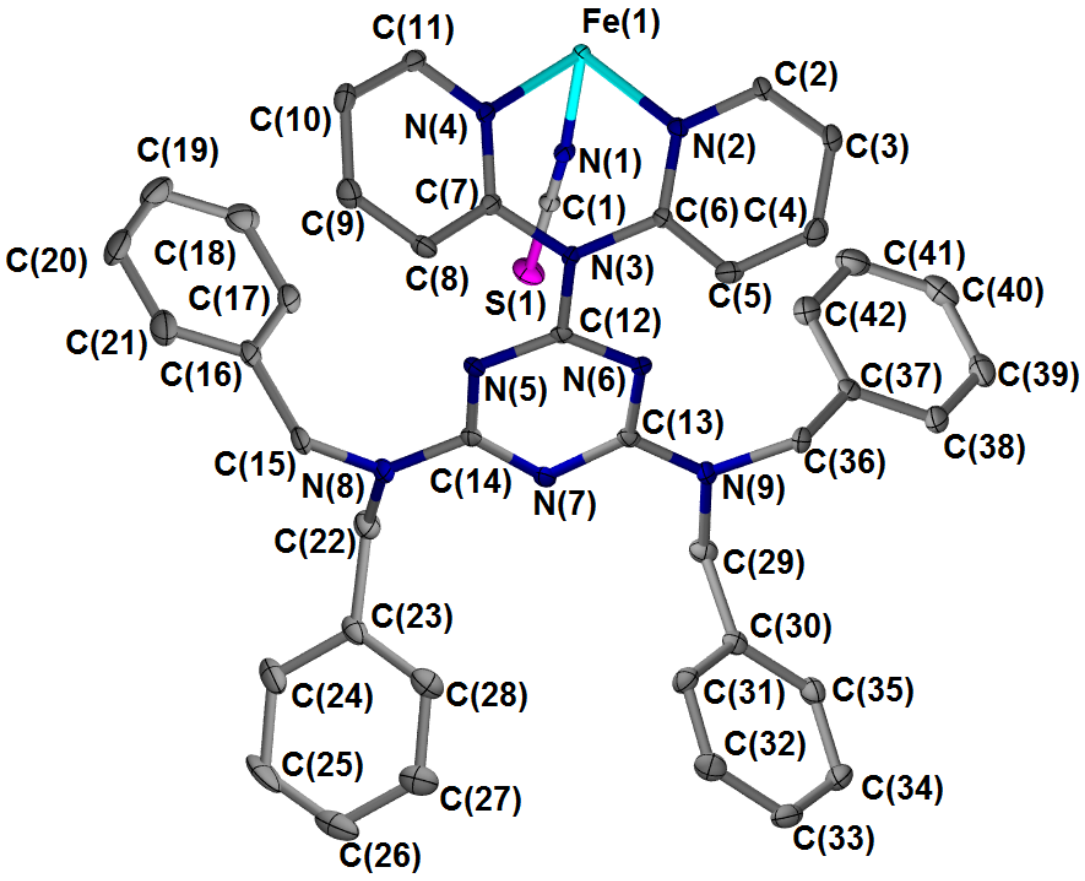

Figure S10 Asymmetric unit of **1a**, showing thermal ellipsoids at 50% probability. Hydrogen atoms have been omitted for clarity.

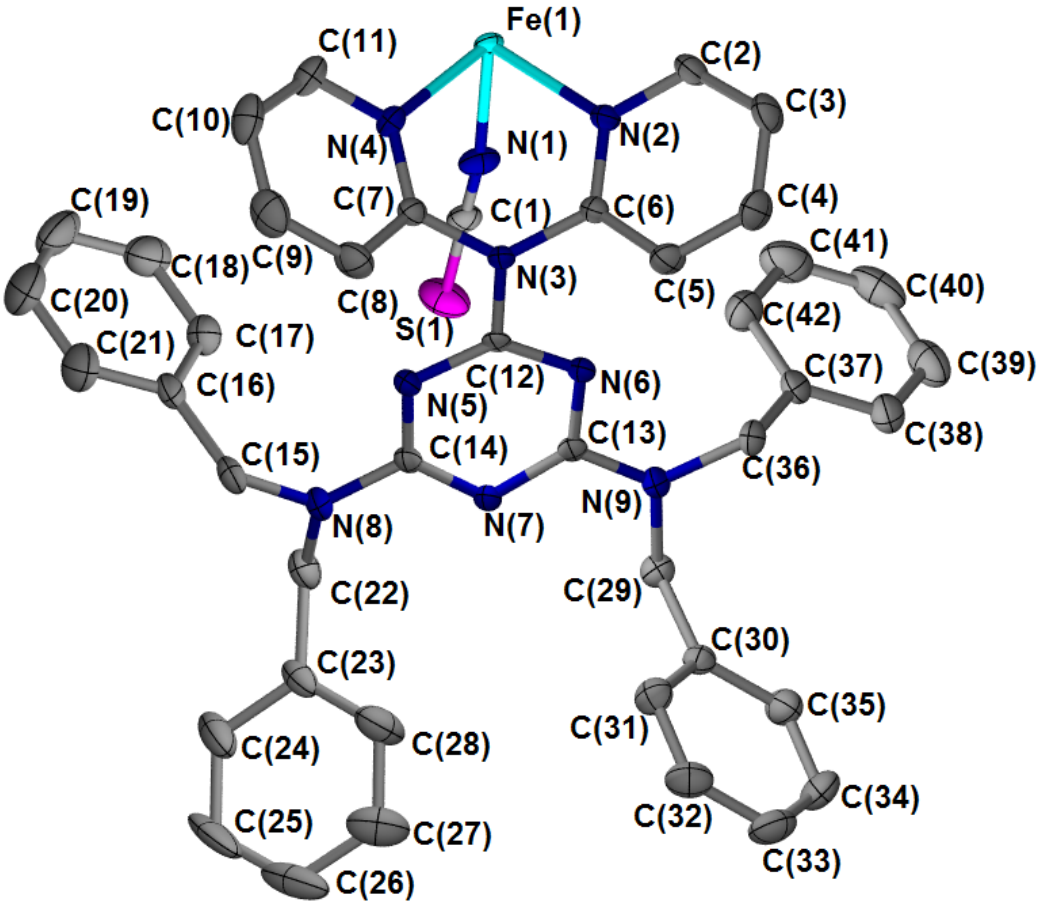

Figure S11 Asymmetric unit of **1b**, showing thermal ellipsoids at 50% probability. Hydrogen atoms have been omitted for clarity.

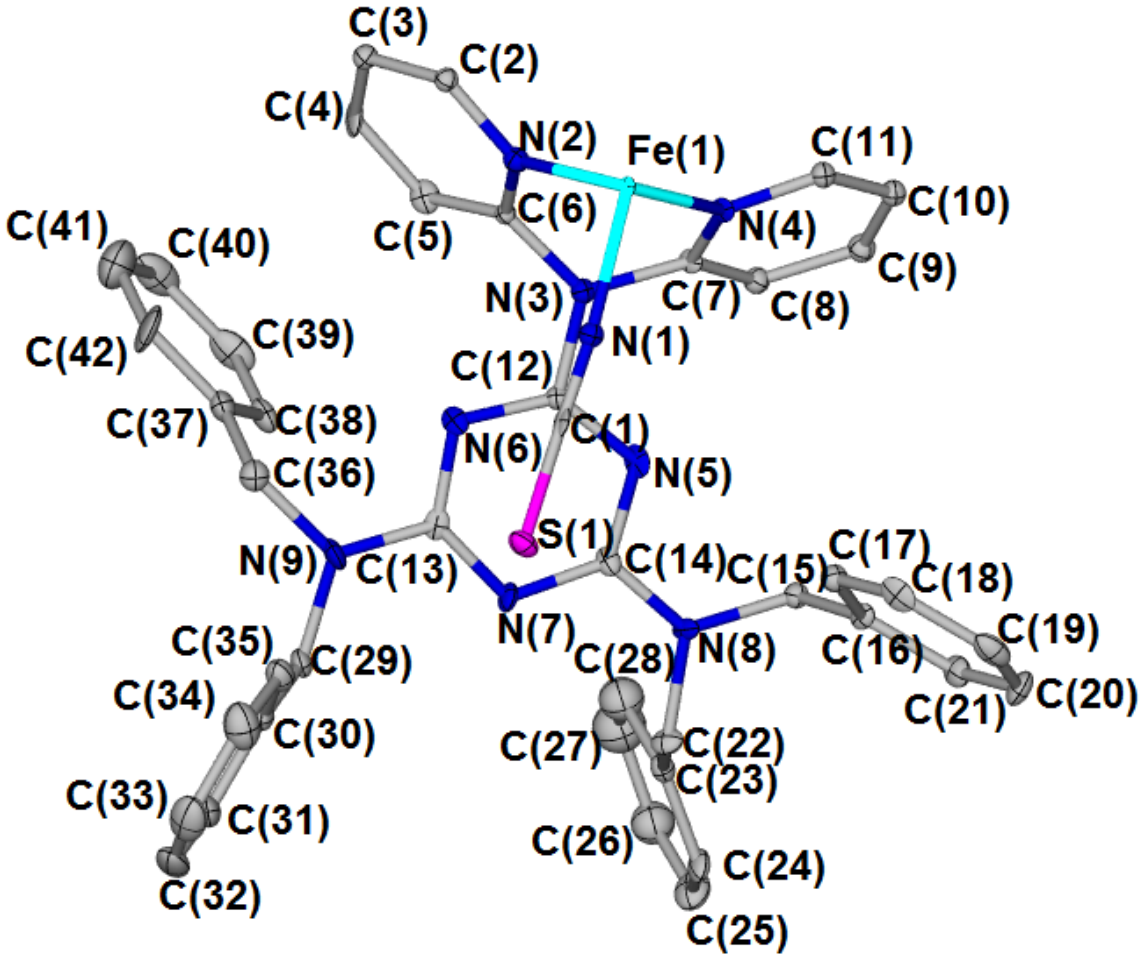

Figure S12 Asymmetric unit of **2**, showing thermal ellipsoids at 50% probability. Hydrogen atoms have been omitted for clarity.

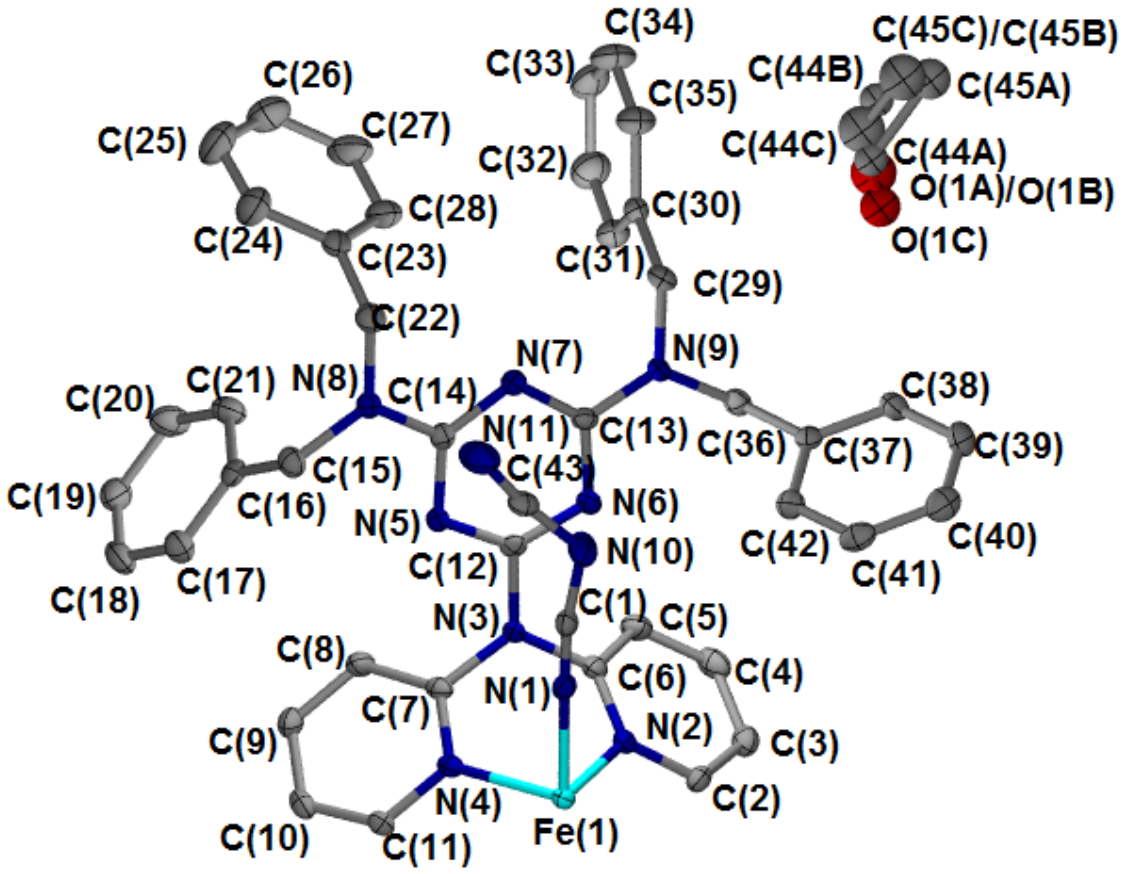

Figure S13 Asymmetric unit of **3**, showing thermal ellipsoids at 50% probability. Hydrogen atoms have been omitted for clarity.

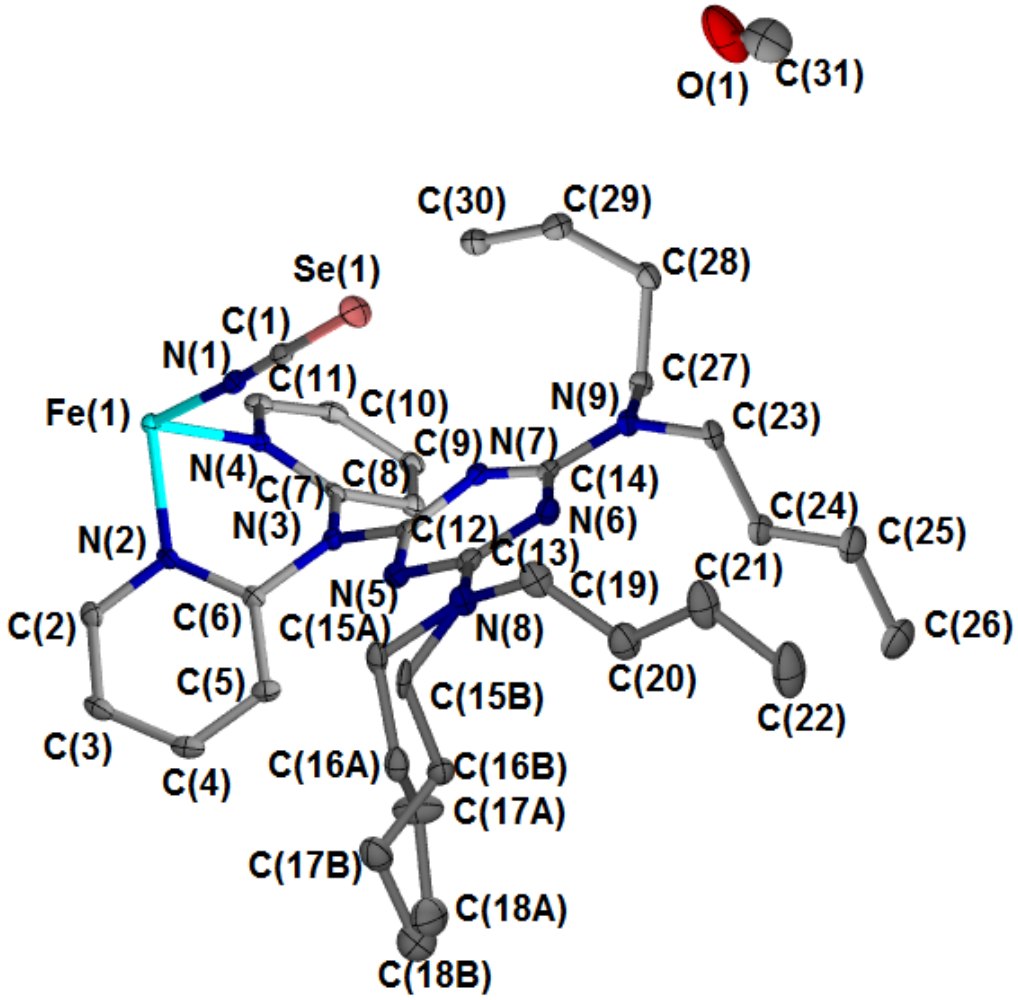

Figure S14 Asymmetric unit of **4**, showing thermal ellipsoids at 50% probability. Hydrogen atoms have been omitted for clarity.

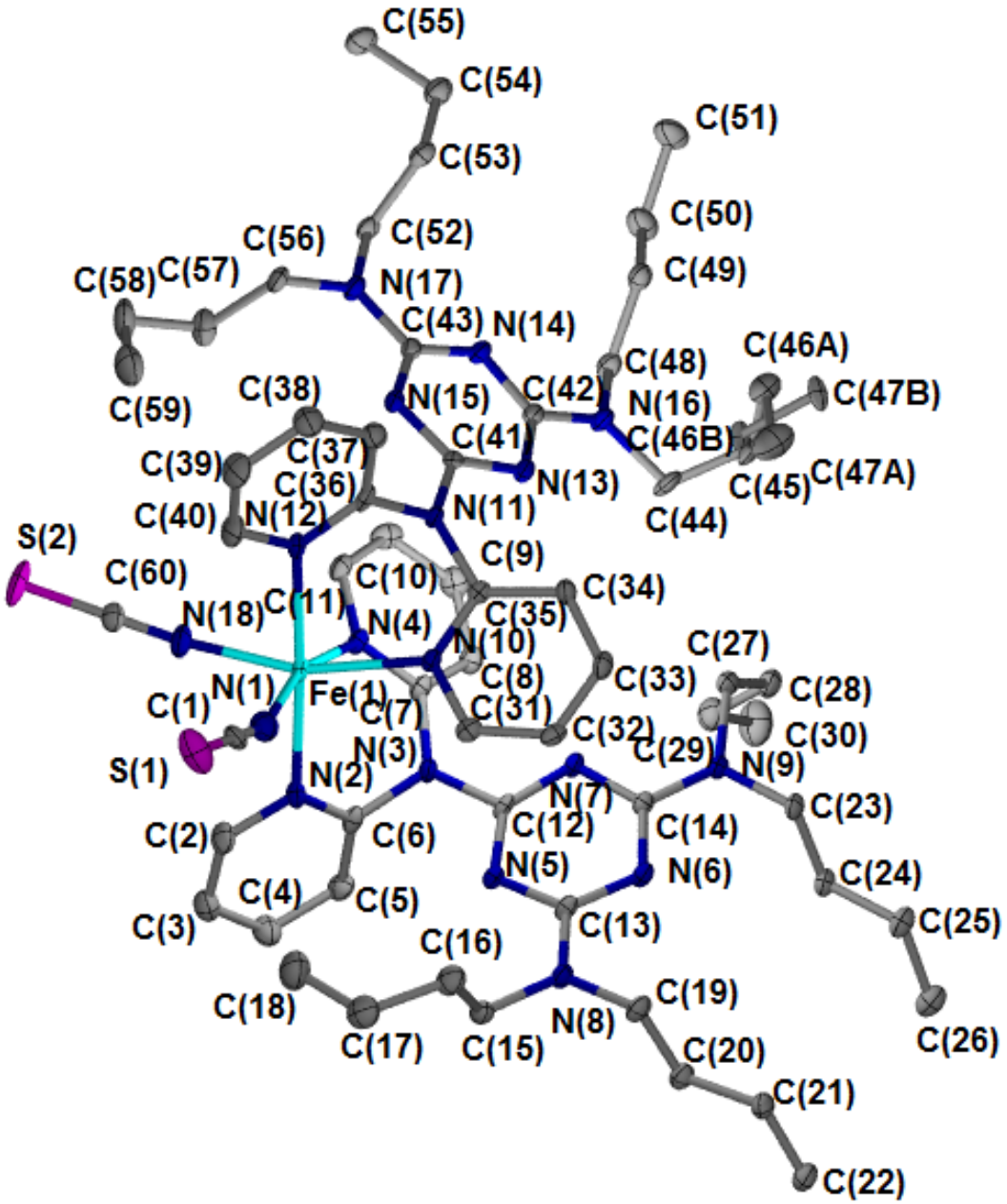

Figure S15 Asymmetric unit of **5**, showing thermal ellipsoids at 50% probability. Hydrogen atoms have been omitted for clarity.

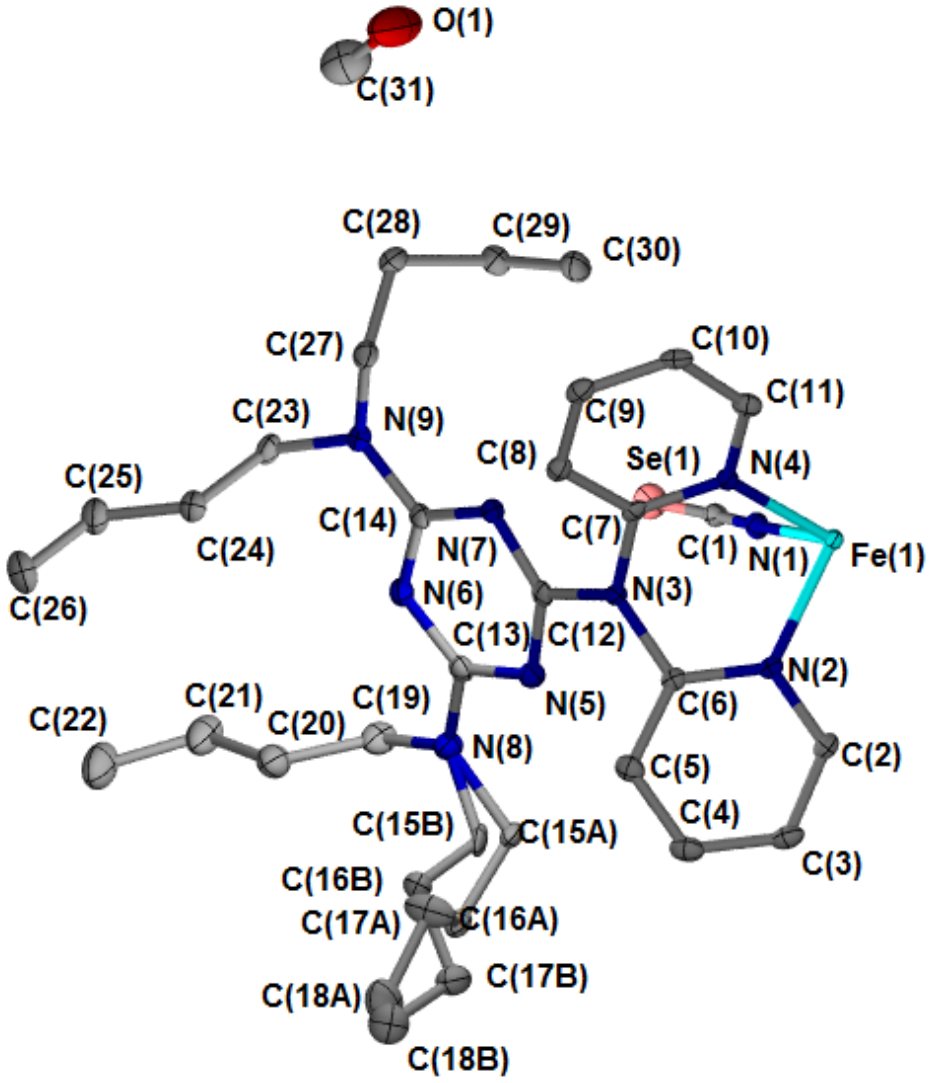

Figure S16 the asymmetric unit for **6**. Atoms are shown at 50% probability. Hydrogen atoms have been omitted for clarity.

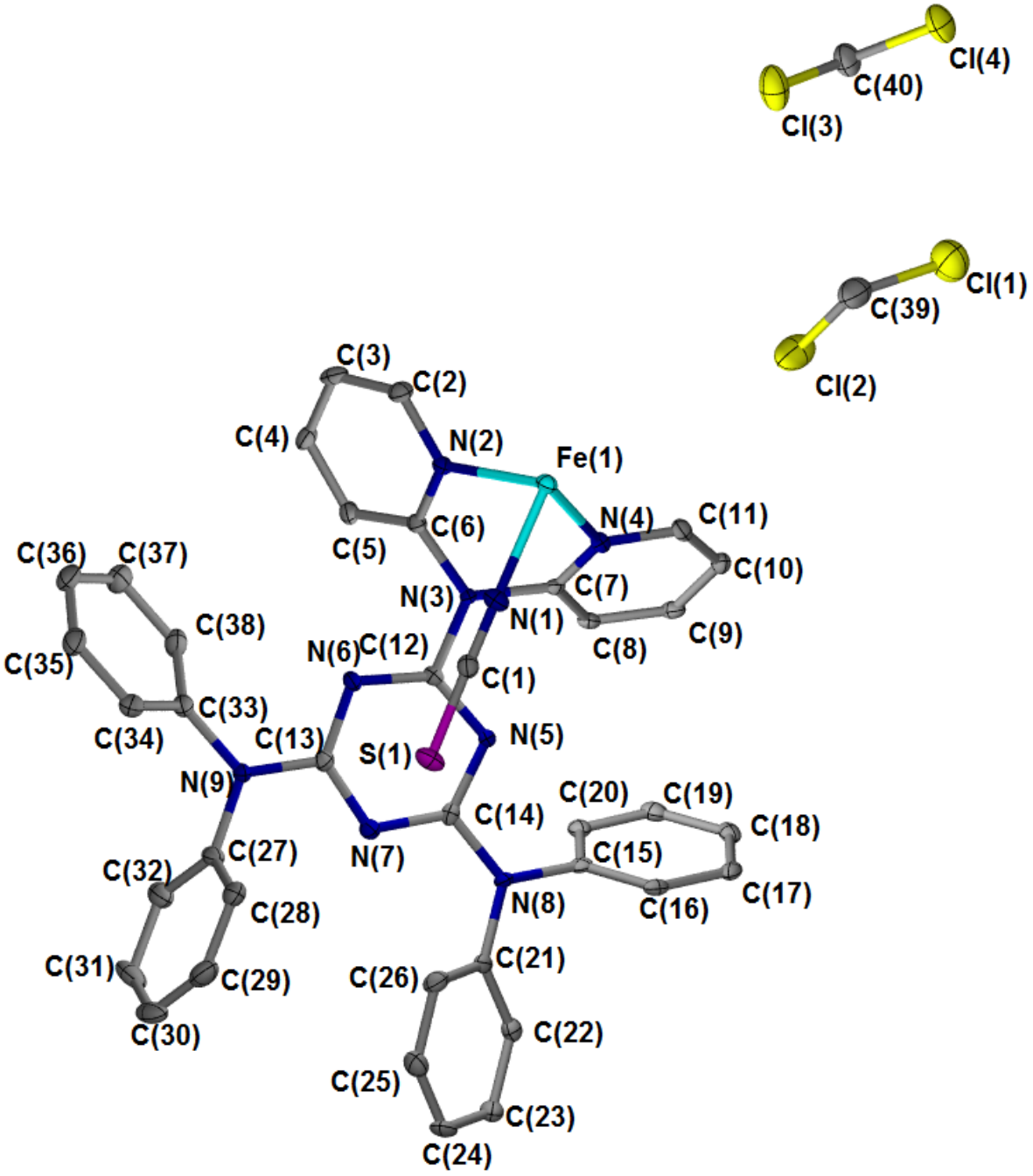

Figure S17 Asymmetric unit of **7**, showing thermal ellipsoids at 50% probability. Hydrogen atoms have been omitted for clarity.

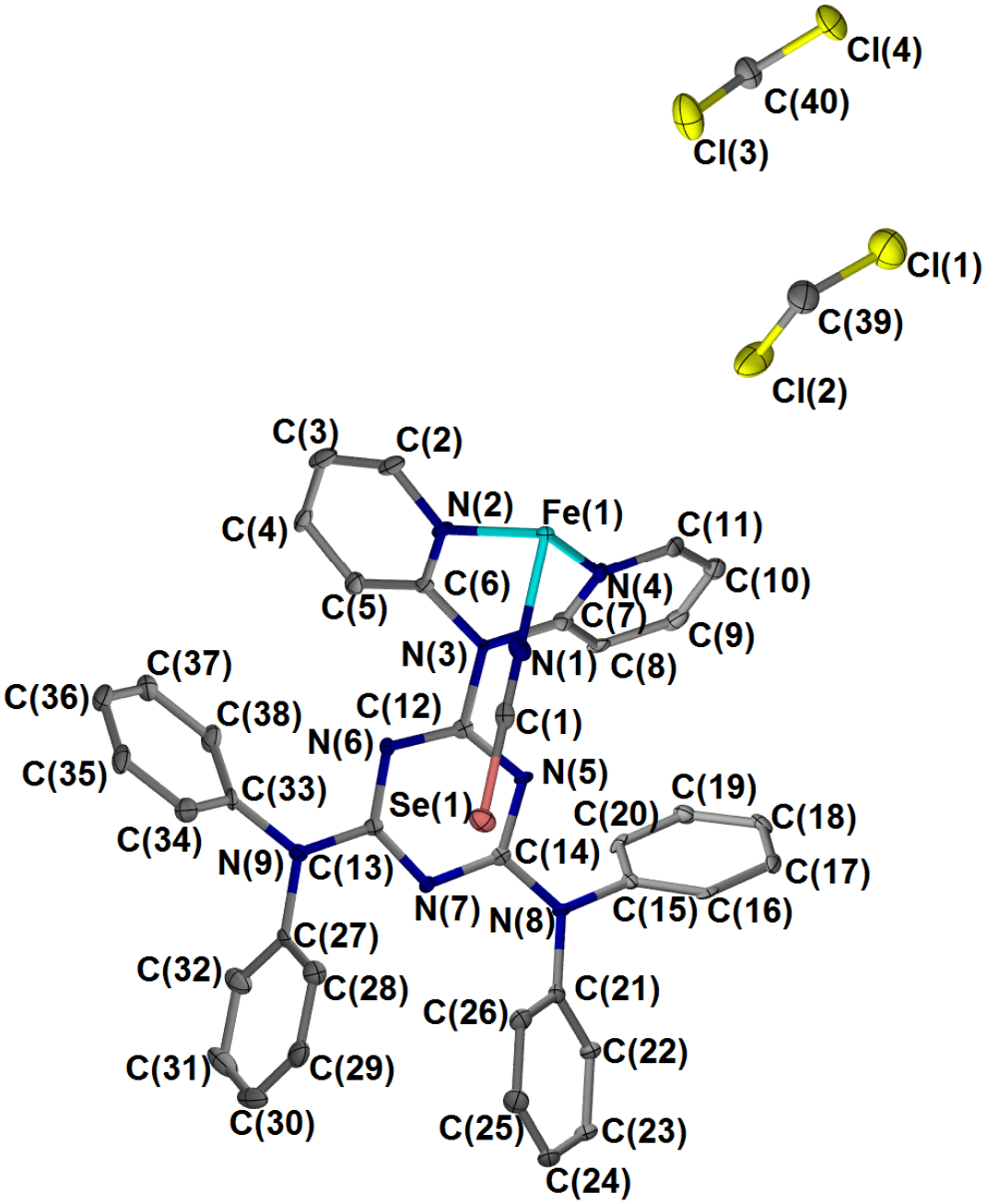

Figure S18 Asymmetric unit of **8**, showing thermal ellipsoids at 50% probability. Hydrogen atoms have been omitted for clarity.

Selected Intermolecular Contacts

Table S1 Selected intermolecular contacts noted in compound **1** (α-*trans*-$[Fe^{II}(NCS)_2(DBB)_2]$)

	1a	**1b**
	100	220
Ω2… Ω3 (Å)[a]	3.773(4) [3.05]	3.819(5) [3.02]
Ω2… Ω5 (Å)[b]	3.379(4)	3.477(4)
Ω4… Ω6a (Å)[c]	3.567(4) [2.95]	3.627(5) [3.02]
Ω5… Ω6a (Å)[d]	3.496(4)	3.577(4)
$H_{Ω5}$…S[e]	3.16	3.16
$H_{Ω3}$…S[f]	3.13	3.17

[a]The distance between C10 and C19 of the monomer generated by symmetry by a one half unit cell length translation in the direction of the *b*-axis, followed by a one half unit cell length translation in the direction of the *c*-axis, , followed by a reflection in a plane parallel to the *b*-*c* plane, constituting an edge-to-face aryl interaction. [the distance between H10 and C19]. [b]The distance between C10 and C33 of the monomer generated by symmetry by a one unit cell length translation in the direction of the *a*-axis, constituting a face-to-face π-stacking interaction. [c]The distance between C28 and C40 of the monomer generated by symmetry by a one unit cell length translation in the direction of the *a*-axis, followed by a one unit cell length translation in the direction of the *c*-axis, constituting an edge-to-face aryl interaction [the distance between H40 and C28]. [d] The distance between C35 and C41 of the monomer generated by symmetry by a one unit cell length translation in the direction of the *a*-axis, followed by a one unit cell-length translation in the direction of the *c*-axis, constituting a face-to-face aryl interaction. [e] Close contact between S1 and H35 of the monomer generated by symmetry by one unit cell length translation in the direction of the *a*-axis, followed by a one unit cell length translation in the direction of the *c*-axis. [f] Closet contact between S1 and H20 of the monomer generated by symmetry by a one half unit cell length translation in the direction of the *b*-axis, followed by a one half unit cell length translation in the direction of the *c*-axis, followed by a reflection in a plane parallel to the *b*-*c* plane.

Table S2 Selected intermolecular contacts noted in compound **2** (β-*trans*-$[Fe^{II}(NCS)_2(DBB)_2]$)

	2
T/K	100
Ω1… Ω3 (Å)[a]	3.27(1)
Ω2… Ω2 (Å)[b]	3.71(2)
Ω4… Ω4 (Å)[c]	3.38(3)
Ω5… Ω6 (Å)[d]	3.71(2) [2.91]
$H_{Ω1}$…S1[e]	2.77
$H_{Ω3}$…S1[f]	3.12

[a]The distance between C3 and C18 of the monomer generated by symmetry by a one unit cell length translation in the direction of the *a*-axis, constituting a face-to-face π-stacking interaction. [b]The distance between C10 and C10 of the monomer generated by symmetry by a one unit cell length translation in the direction of the *b*-axis, possibly constituting a slipped face-to-face π-stacking interaction [c]The distance between C27 and C27 of the monomer generated by symmetry by a one unit cell length translation in the direction of the *b*-axis, followed by a one unit cell length translation in the direction of the *c*-axis, constituting a slipped face-to-face π-stacking interaction. [d]The distance between C31 and C41 of the monomer generated by symmetry by a one unit cell length translation in the direction of the *a*-axis, constituting an edge-to-face aryl interaction [the distance between H41 and C31]. [e] Close contact between S1 and H3 of the monomer generated by symmetry by a one unit cell length translation in the direction of the *a*-axis. [f] Close contact between S1 and H20 of the monomer generated by symmetry by a one unit cell length translation in the direction of the *b*-axis.

Table S3. Selected intermolecular contacts noted in compound **3** (*trans*-$[Fe^{II}(N(CN)_2)_2(DBB)_2]•2CH_3CH_2OH$)

	3
T/K	123
Ω2… Ω6 (Å)[a]	3.343(5)

[a]The distance between C10 and C41 of the monomer generated by symmetry by a translation of one unit cell length in the direction of the a-axis, constituting a face-to-face π-stacking interaction.

Table S4. Selected intermolecular contacts noted in compound **7** (*trans*-[$Fe^{II}(NCS)_2(DDT)_2$]•$4CH_2Cl_2$) and **8** (*trans*-[$Fe^{II}(NCSe)_2(DDT)_2$]•$4CH_2Cl_2$).

	7	**8**
T/K	123	123
Ω2…Ω2 (Å)[a]	3.464(6)	3.475(8)
Ω1…Ω3 (Å)[b]	3.520(4) [2.61]	3.439(6) [2.55]
Ω3…Ω3 (Å)[c]	3.175(4)	3.166(5)
Ω1…Ω4 (Å)[d]	3.641(5) [2.73]	3.624(6) [2.71]
Ω5… Ω6 (Å)[e]	3.644(5) [2.92]	3.663(6) [2.93]

[a]The distance between C8 and C8 of the monomer generated by symmetry by a one unit cell length translation in the direction of the *a*-axis constituting a slipped face-to-face π-stacking interaction. [b]The distance between C2 and C17 of the monomer generated by symmetry by a one unit cell length translation in the direction of the *a*-axis, followed by a one unit cell length translation in the direction of the *b*-axis, constituting a C-H...π aryl interaction [the distance between H2 and C17] . [c]The distance between C16 and C17 of the monomer generated by symmetry by a one unit cell length translation in the direction of the *a*-axis, followed by a one unit cell length translation in the direction of the *b*-axis, constituting a slipped face-to-face π-stacking interaction. [d]The distance between C3 and C22 of the monomer generated by symmetry by a one unit cell length translation in the direction of the *a*-axis, followed by a one unit cell length translation in the direction of the *b*-axis, constituting a C-H...π aryl interaction [the distance between H22 and C3]. [e]The distance between C30 and C35 of the monomer generated by symmetry by a one unit cell length translation in the direction of the *c*-axis constituting a C-H...π aryl interaction [the distance between H35 and C30].

Parallel Quardruple Phenyl Embrace motif within 5 - 8

Within **5** the PQPE motif is adopted between symmetry equivalent DDB ligands on adjacent complex molecules, and in the first case a closest C...C distance of 4.274(5) Å between facially oriented pyridyl rings (with a centroid-to-centroid separation of 4.45 Å) is noted, with a closest C...H distance of 3.55 Å between these and adjacent pyridyl rings and an Fe...Fe separation of 8.786(1) Å (Table 1), while in the second case a closest C...C distance of 4.098(5) Å between facially oriented pyridyl rings (with a centroid-to-centroid separation of 5.30 Å) is noted, with a closest C...H distance of 5.25 Å between these and adjacent pyridyl rings and an Fe...Fe separation of 10.659(1) Å. Within **5** these mutually embracing pyridyl rings are likely too far removed from each other to be classifiable as participating in aromatic interactions. Within the PQPE motif for **6**, the closest C...C distance between the facially oriented pyridyl rings is 3.704(2) Å (the centroid to centroid separation is 3.82 Å), possibly suggesting that no π-stacking interactions are present. Within **6** the PQPE motif contains edge-to-face C-H...π interactions with a closest H...C contact of 2.84 Å noted. Within the extended structures of **7** and **8** the PQPE motif is also observed between pyridyl rings on adjacent complex molecules, but the slipped face-to-face π-stacking interaction occurring as part of this motif in **7** and **8** is more offset than what is noted in **4** (for example, within **7**, the centroid to centroid separation between the parallel pyridyl rings is 4.11 Å, and the closest C...C distance here is 3.464(6) Å). A C-H...π interaction is also observed as part of the PQPE motif in both **7** and **8**, and, here, a closest H...C contact of 2.86 Å is noted.

Table S5. Unit cell parameters for Le Bail fits to powder X-ray diffractograms collected on **1**.

Temperature (K)	*a* (Å)	*b* (Å)	*c* (Å)	*β* (°)	Volume (Å^3)	χ^2
110	11.4823(2)	23.3475(3)	13.5598(1)	96.977(1)	3608.22(8)	2.360
120	11.4844(2)	23.3541(3)	13.5701(1)	96.976(1)	3612.64(8)	2.400
130	11.4877(2)	23.3602(3)	13.5817(1)	96.985(1)	3617.65(8)	2.248
140	11.4934(2)	23.3665(2)	13.5979(1)	97.026(1)	3624.44(8)	2.222
150	11.5021(2)	23.3700(2)	13.6178(1)	97.117(1)	3632.29(8)	2.255
155	11.5087(2)	23.3683(3)	13.6316(1)	97.206(1)	3637.09(8)	2.429
160	11.5164(2)	23.3624(3)	13.6526(1)	97.391(1)	3642.7(1)	2.708
165	11.5333(3)	23.3517(3)	13.6838(2)	97.646(2)	3652.6(1)	3.362
170	11.5502(3)	23.3418(3)	13.7178(2)	97.913(2)	3663.1(1)	4.708
175	11.5673(3)	23.3319(3)	13.7476(2)	98.131(1)	3673.0(1)	4.724
180	11.5792(2)	23.3271(3)	13.7708(1)	98.270(1)	3680.9(1)	4.792
185	11.5869(2)	23.3237(3)	13.7883(1)	98.358(1)	3686.7(1)	5.015
190	11.5927(2)	23.3226(3)	13.8017(1)	98.413(1)	3691.4(1)	5.051
195	11.5976(2)	23.3225(3)	13.8137(1)	98.453(1)	3695.8(1)	5.237
200	11.6024(2)	23.3238(3)	13.8250(1)	98.481(1)	3700.3(1)	5.257
210	11.6086(2)	23.3283(3)	13.8439(1)	98.512(1)	3707.7(1)	5.245
220	11.6138(2)	23.3347(3)	13.8602(1)	98.528(1)	3714.7(1)	5.226
230	11.6185(2)	23.3408(3)	13.8753(1)	98.533(1)	3721.1(1)	5.082
240	11.6225(2)	23.3475(3)	13.8887(1)	98.532(1)	3727.1(1)	6.014
250	11.6258(2)	23.3539(3)	13.9007(1)	98.528(1)	3732.4(1)	6.046

Table S6. Unit cell parameters for Le Bail fits to powder X-ray diffractograms collected on **2**.

Temperature (K)	*a* (Å)	*b* (Å)	*c* (Å)	*α* (°)	*β* (°)	*γ* (°)	Volume (Å^3)	χ^2
200	10.2676(2)	10.4305(2)	20.1343(3)	98.430(1)	92.428(1)	119.1184(8)	1847.3(15)	1.302
210	10.2726(2)	10.4342(2)	20.1455(3)	98.430(1)	92.417(1)	119.1055(8)	1850.1(15)	1.334
220	10.2777(2)	10.4368(2)	20.1580(3)	98.439(1)	92.403(1)	119.0866(9)	1853.0(16)	1.521
230	10.2845(2)	10.4413(2)	20.1724(3)	98.449(1)	92.386(2)	119.065(1)	1856.8(18)	1.791
240	10.2915(2)	10.4450(3)	10.1887(4)	98.449(1)	92.376(2)	119.034(2)	1860.8(19)	2.088
250	10.3002(2)	10.4467(2)	20.2023(3)	98.448(1)	92.356(1)	119.0038(9)	1864.6(16)	1.601
260	10.3116(2)	10.4505(3)	20.2216(4)	98.443(1)	92.333(1)	119.9591(9)	1870.2(16)	1.690
265	10.3174(2)	10.4504(3)	20.2307(4)	98.432(1)	92.325(1)	118.9265(9)	1872.8(16)	1.734
270	10.3245(2)	10.4518(2)	20.2412(4)	98.427(1)	92.309(1)	118.8963(9)	1875.9(17)	1.633
275	10.3314(2)	10.4526(2)	20.2507(3)	98.417(1)	92.292(1)	118.8654(8)	1879.0(15)	1.431
280	10.3388(2)	10.4530(2)	20.2605(3)	98.407(1)	92.279(1)	118.8230(8)	1882.1(16)	1.506
285	10.3464(2)	10.4545(2)	20.2712(4)	98.392(1)	92.270(2)	118.7992(9)	1885.5(17)	1.656
290	10.3543(2)	10.4554(3)	20.2816(4)	98.379(1)	92.255(2)	118.7655(9)	1888.9(18)	1.771
295	10.3622(2)	10.4567(3)	20.2913(4)	98.365(1)	92.240(2)	118.7309(9)	1892.3(19)	1.764
300	10.3699(3)	10.4576(3)	20.3010(4)	98.351(2)	92.226(2)	118.696(1)	1895.6(21)	1.971
310	10.3849(3)	10.4614(3)	20.3202(4)	98.332(2)	92.188(2)	118.634(1)	1902.4(20)	1.895
320	10.3996(3)	10.4654(3)	20.3399(4)	98.314(2)	92.153(2)	118.575(1)	1909.1(20)	1.793
330	10.4151(3)	10.4711(3)	20.3617(5)	98.314(2)	92.104(2)	118.524(1)	1916.2(21)	1.967
340	10.4277(3)	10.4781(3)	20.3795(4)	98.319(2)	92.056(2)	118.480(1)	1922.5(21)	1.949
350	10.4392(2)	10.4856(3)	20.3986(4)	98.339(1)	92.007(2)	118.446(1)	1928.6(19)	1.746
360	10.4498(5)	10.4938(5)	20.417(1)	98.369(1)	91.958(2)	118.4144(9)	1934.4(18)	1.603
370	10.4592(6)	10.5026(6)	20.435(1)	98.404(1)	91.912(2)	118.3881(9)	1939.9(19)	1.703

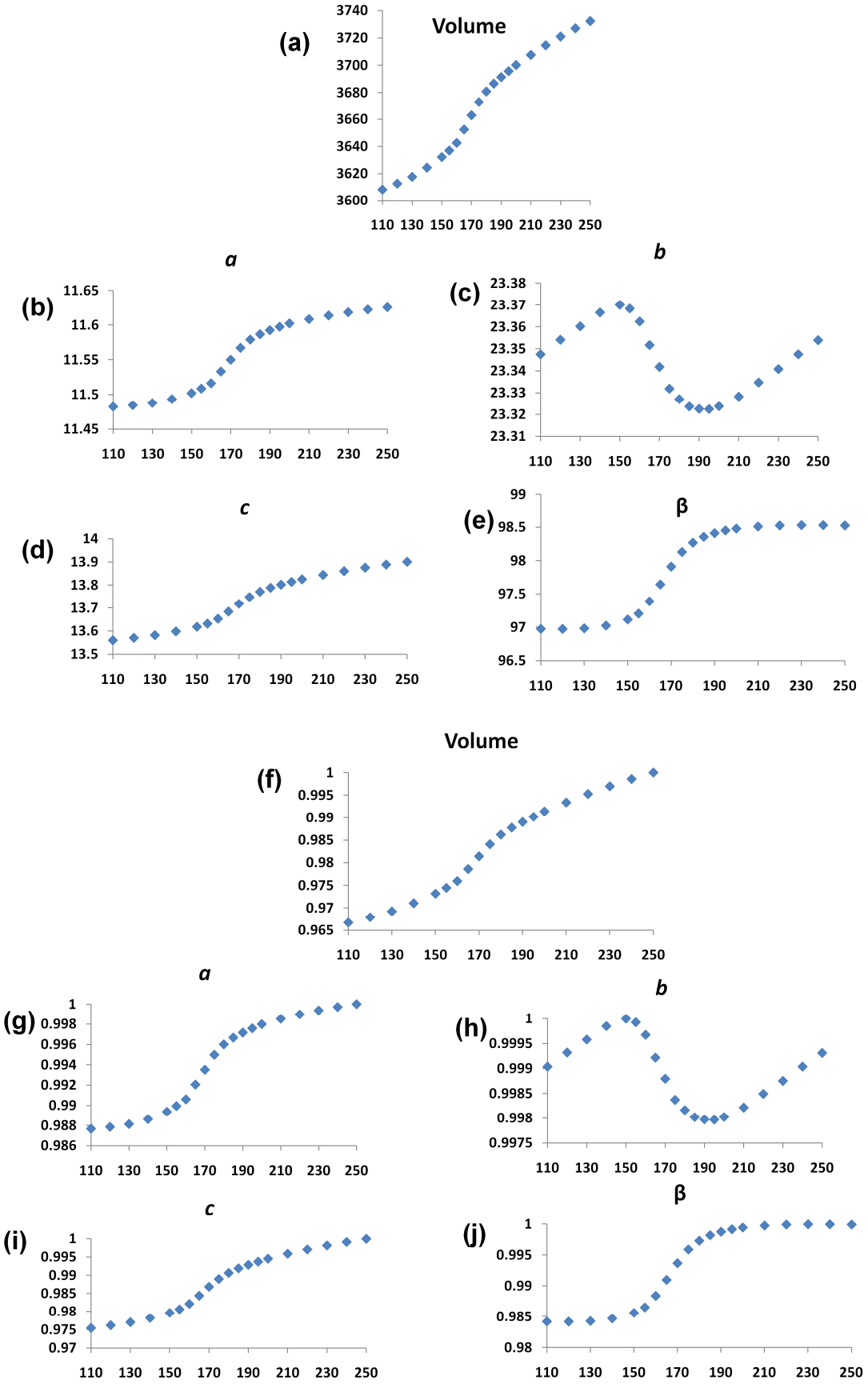
(a)
Volume
3740
3720
3700
3680
3660
3640
3620
3600
110 130 150 170 190 210 230 250
(b)
a
11.65
11.6
11.55
11.5
11.45
110 130 150 170 190 210 230 250
(c)
b
23.38
23.37
23.36
23.35
23.34
23.33
23.32
23.31
110 130 150 170 190 210 230 250
(d)
c
14
13.9
13.8
13.7
13.6
13.5
110 130 150 170 190 210 230 250
(e)
β
99
98.5
98
97.5
97
96.5
110 130 150 170 190 210 230 250
Volume
(f)
1
0.995
0.99
0.985
0.98
0.975
0.97
0.965
110 130 150 170 190 210 230 250
(g)
a
1
0.998
0.996
0.994
0.992
0.99
0.988
0.986
110 130 150 170 190 210 230 250
(h)
b
1
0.9995
0.999
0.9985
0.998
0.9975
110 130 150 170 190 210 230 250
(i)
c
1
0.995
0.99
0.985
0.98
0.975
0.97
110 130 150 170 190 210 230 250
(j)
β
1
0.995
0.99
0.985
0.98
110 130 150 170 190 210 230 250

Figure S19 (shown on previous page) **(a)** Temperature dependent behaviour of the unit cell volume for **1**; **(b)** temperature dependent behaviour of *a* for **1**; **(c)** temperature dependent behaviour of *b* for **1**; **(d)** temperature dependent behaviour of *c* for **1**; **(e)** temperature dependent behaviour of the angle β for **1**; **(f)** temperature dependent behaviour of the unit cell volume for **1** given as a proportion of its highest magnitude; **(g)** temperature dependent behaviour of *a* for **1** given as a proportion of its highest magnitude; **(h)** temperature dependent behaviour of *b* for **1** given as a proportion of its highest magnitude; **(i)** temperature dependent behaviour of *c* for **1** given as a proportion of its highest magnitude; **(j)** temperature dependent behaviour of the angle β for **1** given as a proportion of its highest magnitude. In all Figures the horizontal axis is temperature (given in K), while in Figure **(a)** the vertical axis is given in $Å^3$, in Figures **(b)**, **(c)** and **(d)** the vertical axis is given in Å, for **(e)** the vertical axis is given in ^{o}, and in **(f)** – **(j)** the vertical axis is the proportion of the highest magnitude of the relevant parameter. For Figures **(a)** to **(e)** error bars are given to three times the calculated error, but are eclipsed by the position markers; no error bars are given for **(f)** - **(j)**.

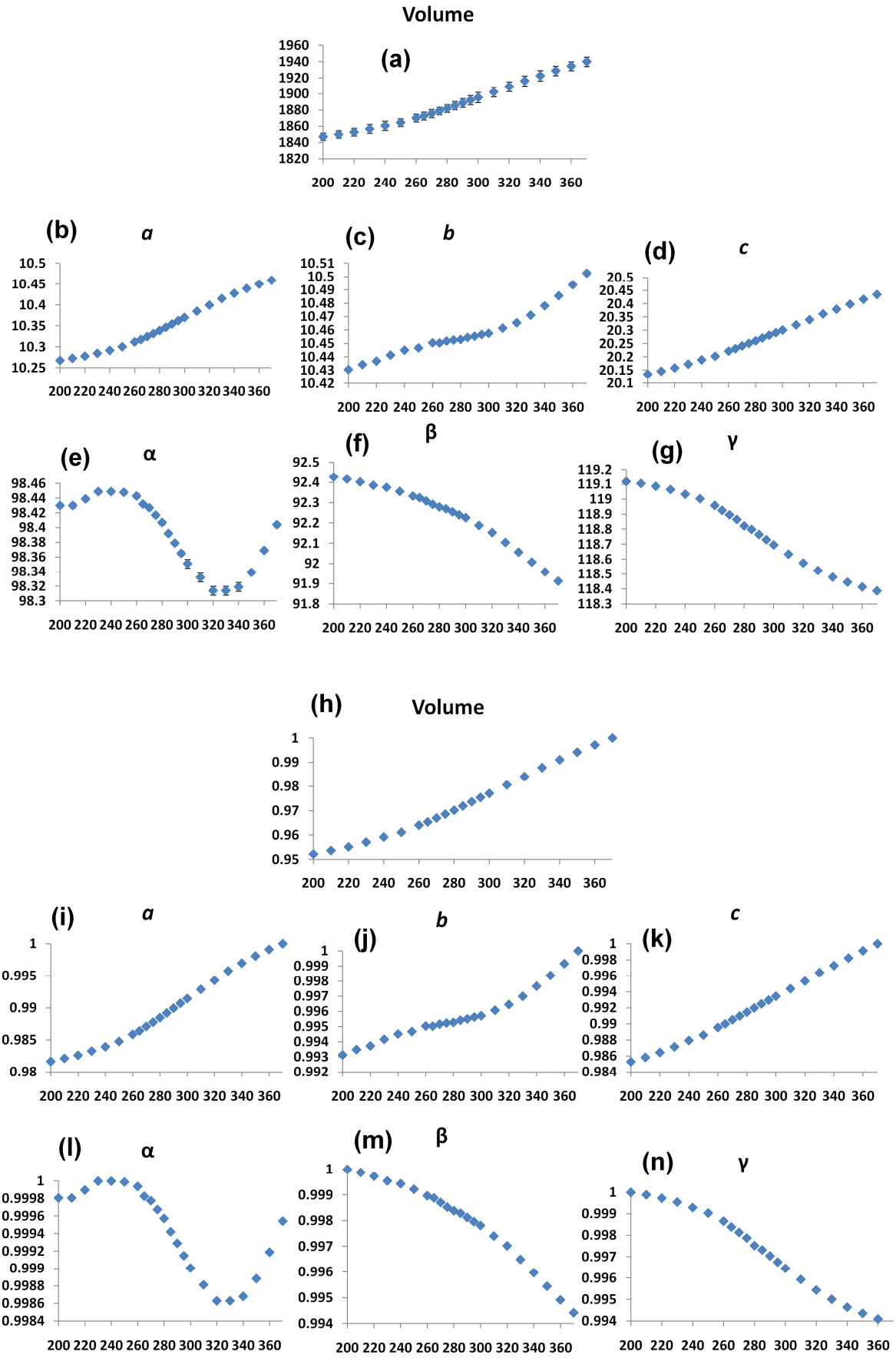
Volume
(a)
(b) a
(c) b
(d) c
(e) α
(f) β
(g) γ
(h) Volume
(i) a
(j) b
(k) c
(l) α
(m) β
(n) γ

Figure S20 (shown on previous page) **(a)** Temperature dependent behaviour of the unit cell volume for **2**; **(b)** temperature dependent behaviour of *a* for **2**; **(c)** temperature dependent behaviour of *b* for **2**; **(d)** temperature dependent behaviour of *c* for **2**; **(e)** temperature dependent behaviour of the angle α for **2**; **(f)** temperature dependent behaviour of the angle β for **2**; **(g)** temperature dependent behaviour of the angle γ for **2**; **(h)** temperature dependent behaviour of the unit cell volume for **2** given as a proportion of its highest magnitude; **(i)** temperature dependent behaviour of *a* for **2** given as a proportion of its highest magnitude; **(j)** temperature dependent behaviour of *b* for **2** given as a proportion of its highest magnitude; **(k)** temperature dependent behaviour of *c* for **2** given as a proportion of its highest magnitude; **(l)** temperature dependent behaviour of the angle α for **2** given as a proportion of its highest magnitude. **(m)** temperature dependent behaviour of the angle β for **2** given as a proportion of its highest magnitude. **(n)** temperature dependent behaviour of the angle γ for **2** given as a proportion of its highest magnitude. In all Figures the horizontal axis is temperature (given in K), while in Figure **(a)** the vertical axis is given in $Å^3$, in Figures **(b)** - **(d)** the vertical axis is given in Å, for **(e)** – **(g)** the vertical axis is given in ^{o}, and in **(h)** – **(n)** the vertical axis is the proportion of the highest magnitude of the relevant parameter. For Figures **(a)** to **(g)** error bars to three times the calculated error are given, but in some cases are eclipsed by the position markers; no error bars are given for **(h)** - **(n)**.

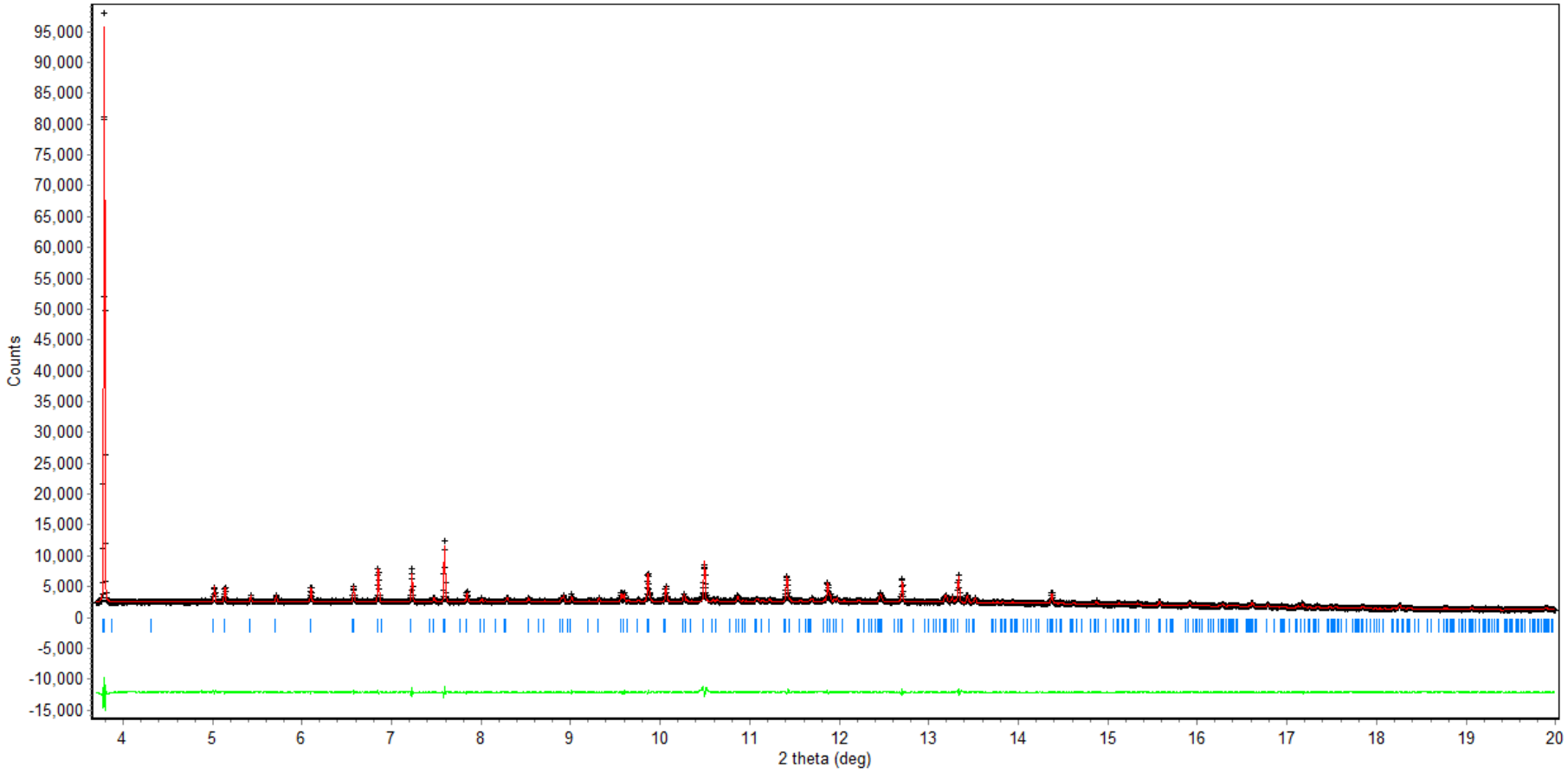

Figure S21 Le Bail fit for powder X-Ray data collected on **1** at 110 K. The black markers are the observed data, the red is the calculated fit to the data, the blue markers represent the predicted peak placement, and the green line is the difference between the observed and calculated data.

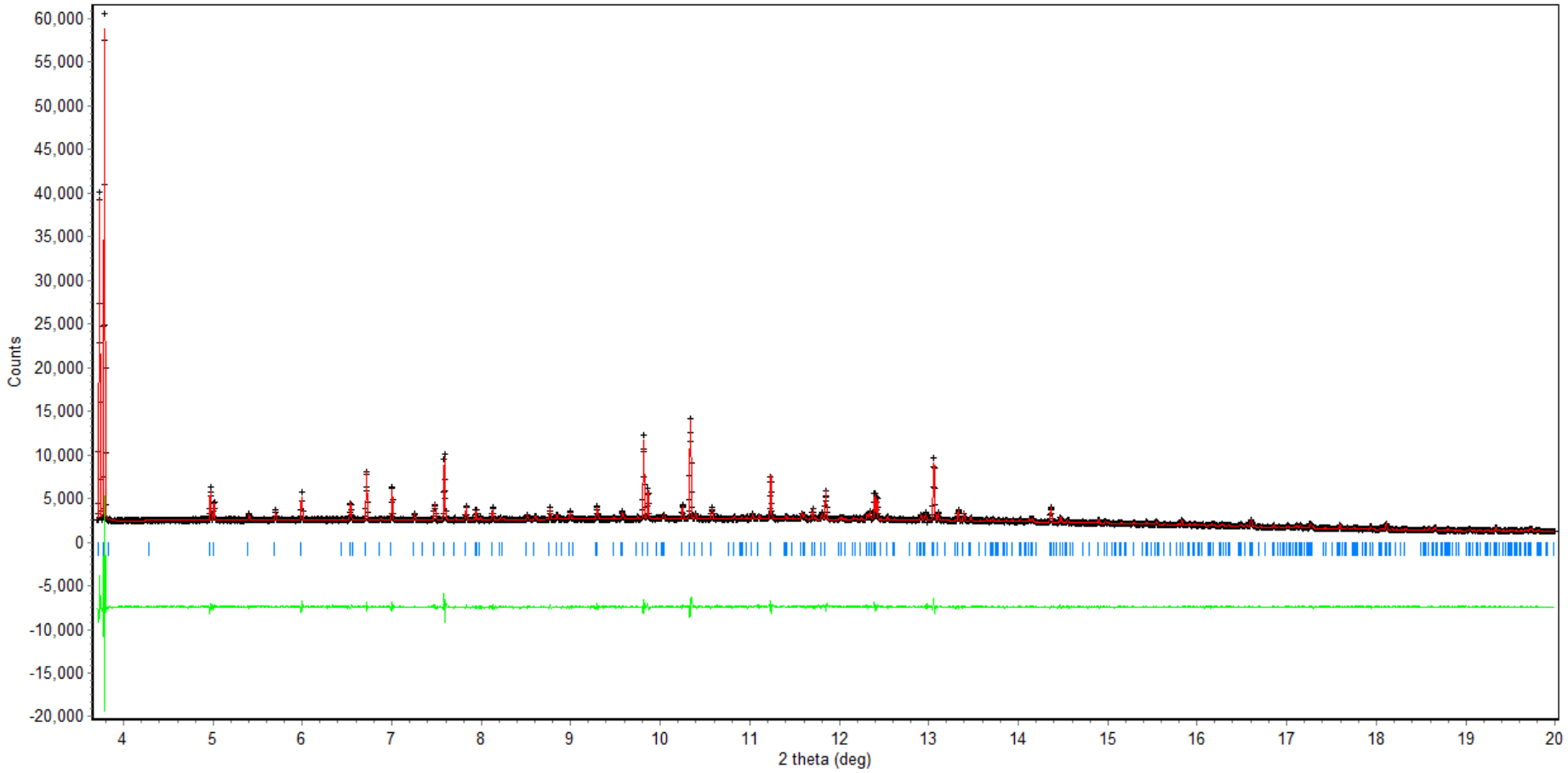

Figure S22 Le Bail fit for powder X-Ray data collected on **1** at 250 K. The black markers are the observed data, the red is the calculated fit to the data, the blue markers represent the predicted peak placement, and the green line is the difference between the observed and calculated data.

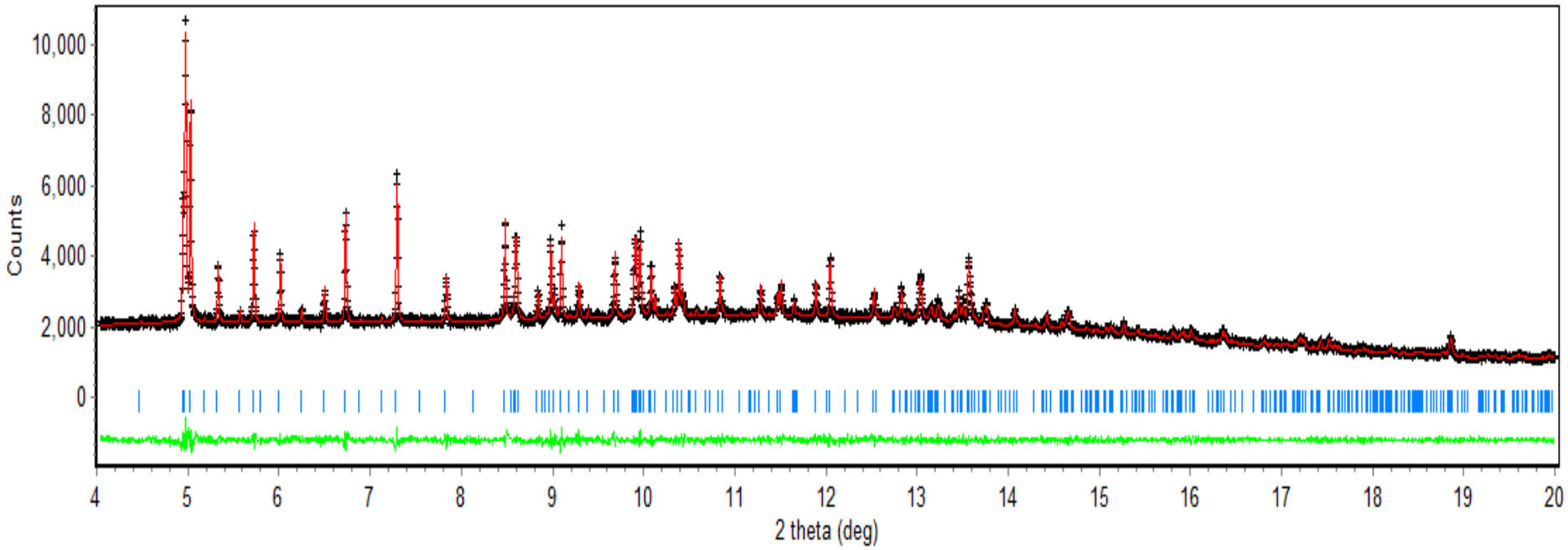

Figure S23 Le Bail fit for powder X-Ray data collected on **2** at 200 K. The black markers are the observed data, the red is the calculated fit to the data, the blue markers represent the predicted peak placement, and the green line is the difference between the observed and calculated data.

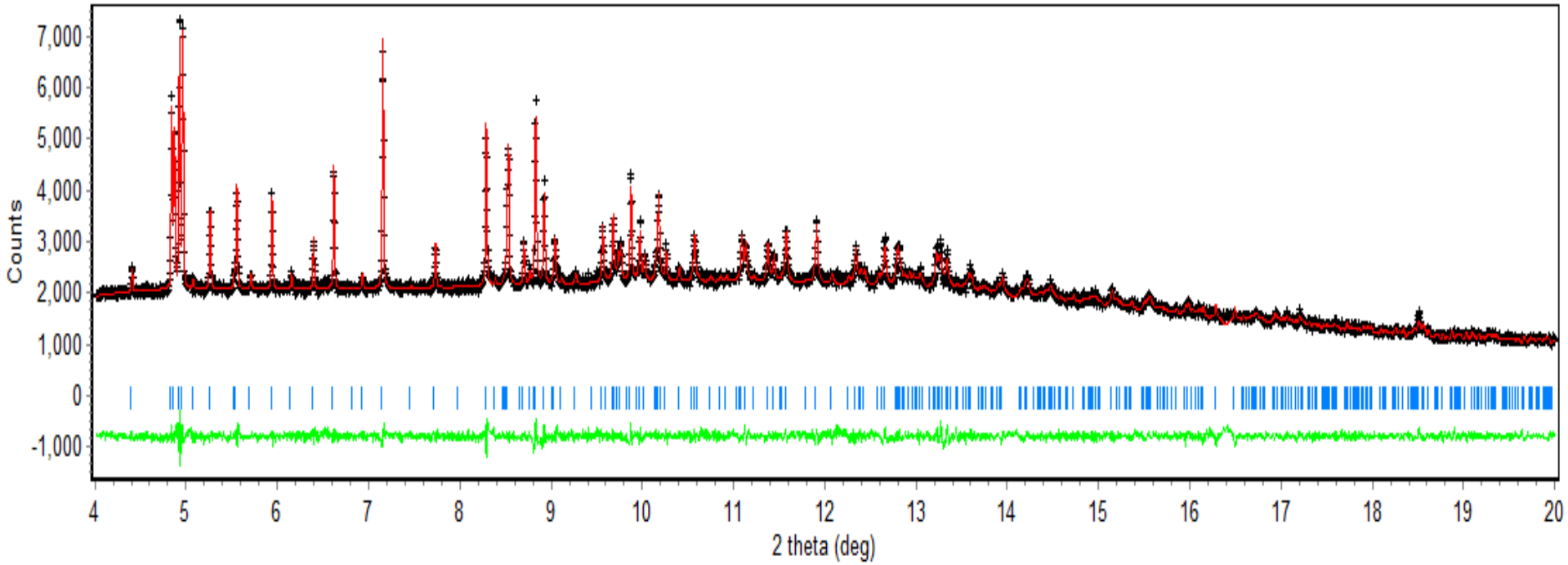

Figure S24 Le Bail fit for powder X-Ray data collected on **2** at 370 K. The black markers are the observed data, the red is the calculated fit to the data, the blue markers represent the predicted peak placement, and the green line is the difference between the observed and calculated data.